Checkerboard-like structure in columnar W-Mo thin films

Nicolas Martin, Jean-Marc Cote, Houssem Boukhalfa, Valérie Potin

Functional Materials Letters
Vol. 5, No. 6 (2015) 2251043
https://doi.org/10.1142/S1793604722510432

Checkerboard-like structure in columnar W-Mo thin films

Nicolas MARTIN*, Jean-Marc COTE
Institut FEMTO-ST, UMR 6174 CNRS Univ. Bourgogne Franche-Comté, 15B, Avenue montboucons, 25030 Besançon Cedex, France

Houssem BOUKHALFA, Valérie POTIN
ICB - Laboratoire Interdisciplinaire Carnot de Bourgogne, UMR 6303 CNRS Univ. Bourgogne Franche-Comté, 9, Avenue Alain Savary, BP47870, 21078 Dijon Cedex, France

Implementing bottom-up approaches to control the columnar architecture of thin films at the nanoscale is a powerful tool for developing surface properties. While inclined columns, zigzags or helices made of a single material are now commonly produced by oblique angle deposition processes, the creation of more complex and original structures associating at least two different materials still remains a challenging task, even more on silicon substrate. Herein, we show how to prepare tungsten/molybdenum columns exhibiting a checkerboard-like structure with motifs of a few tens nanometers. Although understanding the growth phenomena becomes more problematic when two components are simultaneously provided during the film fabrication, this original combination of controlled mosaics in columnar thin films enables new opportunities to produce some unusual nanostructures for functional materials.

Keywords: Nanostructural materials, thin films, sputtering, interfaces, scanning/transmission electron microscopy.

1. Introduction

In the last decades, tremendous efforts have been made to create new architectures in thin films prepared by bottom-up approaches[1,2], especially by sputtering processes[3-6]. Nanostructured thin films with unusual architectures are of broad scientific and technological significance, particularly, for understanding their behaviors at the nanometer scale, but also for their usage in various fields of application. Whatever the fabrication approach, the motivation is to succeed in growing thin films exhibiting original structures with sizes and thicknesses ranging from a few tens to a few hundreds of nanometers. Many materials are smartly prepared with dimensions from the atomic scale[7-9] (e.g., clusters, molecules with chiral structures …) and up to the microscale[10-12] (e.g., self-organized colloidal balls, nacre …). However, between these two ranges of dimensions, a lack of knowledge still remains to be explored, especially about the fabrication of structured materials involving at least two components. Therefore, the development of a toolbox gathering advanced structuring methods is becoming a scientific requirement. Such methods are connected to technological challenges to achieve innovative architectured thin films at these scales. Proceeding and understanding mechanisms of these structuration strategies are one of the motivations of this work.

These last 25 years have seen extensive investigations devoted to the glancing angle deposition (GLAD)[13] since it appears to be an attractive approach to obtain nanostructured thin films[14]. Brett *et al.* acted as pioneers to develop this original way leading to 1D, 2D or 3D structuring[15]. The direct impact of these nanostructured thin films was an extension of many physical properties of such films compared to those obtained with conventional processes[16,17]. Although ability of the films structure by the GLAD technique with a single material is still an attractive method to achieve nanoscale engineering, the GLAD co-deposition extends nanostructuring capabilities.

We report on the preparation of checkerboard-like structure in tungsten-molybdenum thin films co-sputter-deposited by GLAD involving two opposite atomic sources of W and Mo. Each source is inclined with the same tilt angle of 80° relative to the normal of the substrate surface. Tuning judiciously W and Mo particle fluxes, and by means of rapid 180° rotations of the substrate after fixed growth intervals,

* Email: nicolas.martin@femto-st.fr

vertical columns exhibiting checkerboard-like shapes can be produced. These as-deposited columns are composed of clear W/Mo alternations with a tunable patchwork design depending on particle fluxes and frequency of the substrate rotation. Growth mechanisms specific to GLAD process involving W and Mo and co-sputtering conditions also influence the final figure of the columns network. Finer analyses by high-resolution transmission electron microscopy lead to identify a mixture of mainly α– W but also β– W phase and of pure body-centered cubic (bcc) Mo. They also show that during the two metals growth, frank W/Mo interfaces are produced following the columns axis despite inhomogeneous aspects of the columns cross-section.

2. Material and methods

W-Mo films were deposited onto (100) Si substrates by DC reactive magnetron sputtering from two metallic targets (W and Mo purity 99.6 at. % and 51 mm diameter) in an Ar atmosphere. Pumping unit led to a residual vacuum below 10^{-5} Pa before starting any deposition. All depositions were performed with an argon flow rate of 2 sccm leading to a pressure of 0.30 Pa. Targets were sputtered with a constant current density J_W = 140 A m^{-2}, and J_{Mo} = 200 A m^{-2} for W and Mo, respectively. Distances between targets and unheated substrate were fixed at 65 mm for W and 95 mm for Mo. A homemade GLAD substrate-holder allowed the preparation of vertical columns keeping the deposition angles $\alpha_W = \alpha_{Mo} = 80°$. Rotating the substrate holder at $\phi = 180°$ after a given time allowed the creation of checkerboard-like architecture inside columns. The total deposition time was adjusted in order to get 1 to 1.4 µm films thickness.

Top and cross-sectional observations by scanning electron microscopy (SEM) were performed with a JEOL JSM 7600F. The finer structural analysis was completed using a JEOL 2100 FEG transmission electron microscope (TEM) operating at 200 keV. Before TEM observations, samples were prepared by the standard sandwich technique. TEM observations were performed using GATAN Digital Micrograph software and their simulations were obtained with the Java Electron Microscopy Software (JEMS). The elemental chemical composition was also measured in scanning (STEM) mode using an EDX detector BRUKER Quantax XFlash 5030T SDD.

3. Results and discussion

The GLAD process involving a single source has become a well-redounded method since a wide range of nanostructures can be obtained playing with only two key parameters: The deposition angle α (angle between the substrate normal and the incident vapor flux direction), and the angle ϕ measuring the substrate rotation about its normal. Since the 1997 article published by Robbie and Brett[13], many investigations have been devoted to the development of original GLAD film's nanostructures with one vapor source but till now, a very few studies involving at least two sources have been reported[18-22]. The geometry of the sputtering set-up is the starting key parameter to generate the fabrication of complex architectures (e.g., Janus-like structure). A schematic view of our GLAD co-sputtering system is given in figure 1.

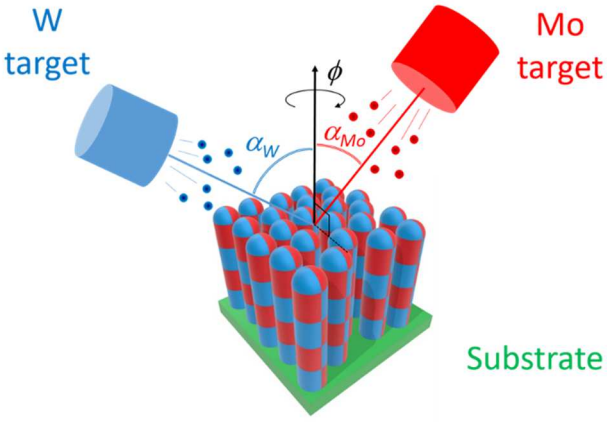

Fig. 1. Schematic illustration of the GLAD co-sputtering system implemented to deposit W-Mo thin films exhibiting a checkerboard-like structure. W and Mo targets are both tilted with a constant angle $\alpha_W = \alpha_{Mo}$ = 80°. Azimuthal angle ϕ can be periodically changed following a sequential rotation of the substrate holder (intermittent 180° ϕ rotations) leading to W/Mo alternations in columns. By an accurate adjustment of W and Mo incoming vapor fluxes, a vertical growth of the columns can be reached.

Both targets are facing to each other and deposition angles α_W and α_{Mo} are fixed at 80°. Such a symmetric configuration and grazing angles are operating parameters favoring the shadowing mechanism[15]. The latter causes the condensing vapor incoming from a target to self-assemble into oriented columns. Combining two sources leads to a growth competition of W and Mo nuclei and bi-metallic columns can develop by means of a careful adjustment of each particle flux (i.e., target current intensities) and a ballistic regime (low sputtering pressure). It is worth noting that these operations conditions have been previously optimized to produce well-defined Janus-like structures playing with sputtering pressure, target current intensity and film's thickness[23]. With a sequential rotation of the substrate holder (intermittent 180° ϕ rotations at each step), the GLAD co-sputtering provides W-Mo films exhibiting checkerboard patterned columns. This arrangement can be tuned assuming

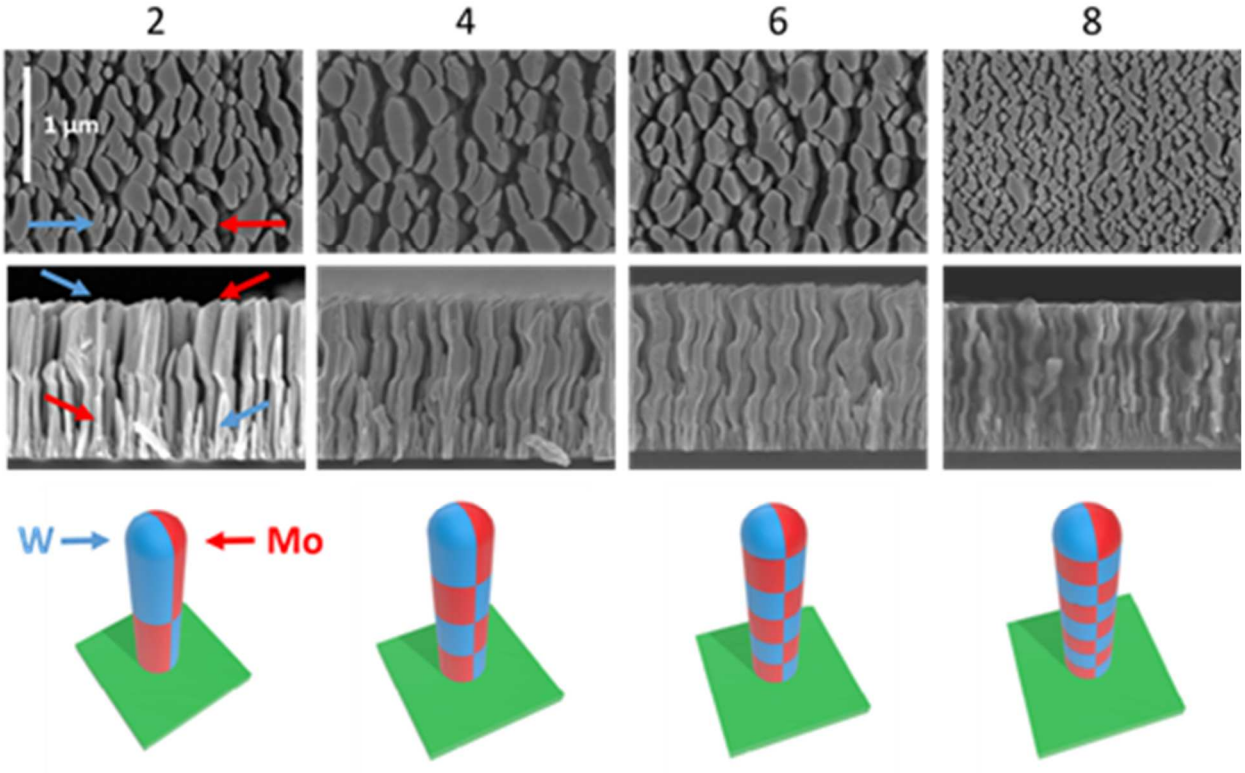

Fig. 2. Top and cross-section observations by SEM of W-Mo thin films co-sputter-deposited with 1, 3, 5 and 7 180° ϕ rotations (corresponding to 2, 4, 6 and 8 alternations). The bar scale is the same for all pictures. For each structure and a single column, W and Mo metals are schematically represented in blue and red, respectively.

W and Mo deposition rates and playing with deposition time of each sequence.

This growth optimization by GLAD co-sputtering allows the preparation of various W-Mo checkerboard structures as shown from SEM observations (Fig. 2). Keeping nearly the same films thickness, 1, 3, 5 and 7 180° ϕ rotations have been performed (leading to 2, 4, 6 and 8 W/Mo alternations, respectively).

All top views (Fig. 2) show a pronounced elongation of the column cross-section in the direction perpendicular to W and Mo particle fluxes. This anisotropic microstructure is typically encountered in GLAD films produced with a single source and mainly assigned to shadowing asymmetry intrinsic to the GLAD process (becoming especially significant at grazing angle > 70°). While the ballistic shadowing mechanism acts following the particle flux direction, there is no mechanism preventing the transverse growth of the column cross-section. An elliptical shape is then produced with a fanning phenomenon of an individual column and thus a chaining of neighbored columns[24]. Implementation of two facing sources with nearly balanced vapor fluxes emphasizes this fan-like columnar structure and so, this anisotropic morphology. Indeed simultaneous head-on fluxes of W and Mo atoms incoming from two opposite directions favors a growth competition between W and Mo columns. Increasing the number of sequential rotations (especially from 5 to 7) gives rise to smaller elliptical cross-sections and thinner spaces between columns. These reduced dimensions are mainly connected to the narrower columns as observed from the cross-section view of the 8 alternations film (Fig. 2). A decrease of deposition time disturbs the column broadening effect observed in GLAD structures, where the column width gradually increases with film thickness. Each 180° ϕ rotation interrupts the regular growth of the columns and the classical power-law dependence of the column width *vs.* film thickness becomes less relevant[25].

For the lowest numbers of ϕ rotations (1 and 3, i.e., 2 and 4 alternations, respectively), it is interesting to note a better-defined columnar structure with serrated column profiles. These dissymmetric profiles correspond to larger parts of W than Mo for a given column. It means that W flux prevails over that of Mo, which agrees with W-rich films (concentrations from STEM-EDX are 68-77 and 23-32 at. % for W and Mo, respectively). It is also worth noting that a large part of the column apex is flat and tilted for sides facing

the W target, which is particularly noticeable for 2 and 4 alternations and corresponds to the W material.

TEM observations performed on the 1 rotation W/Mo films clearly exhibit the checkerboard-like architecture produced by GLAD co-sputtering (Fig. 3).

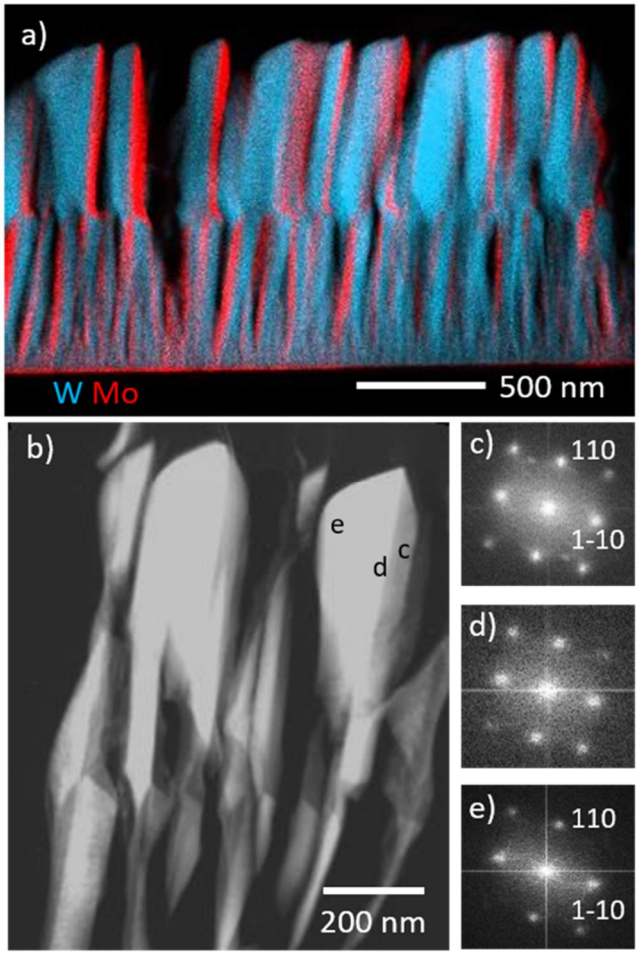

Fig. 3. TEM experiments performed on the 1 rotation W/Mo sample: a) Color-mixed map extracted from dark-field STEM-EDX with W in blue and Mo in red, b) dark-field STEM image with localization of c), d) and e) corresponding FFT patterns. All patterns correspond to the [001] body-centered cubic zone axis (α-phase of W and Mo) with the <110> growth direction.

The two-component columnar structure (Janus-like) is obtained from the first growing stage. The color-mixed map obtained from dark-field STEM-EDX shows W/Mo alternations with a majority of W (blue in Fig. 3a). This corroborates with the W-rich films obtained from the compositional analysis previously reported and the predominance of W during the columnar growth. The facet angle of the column apex related to the W material is again clearly visible and frank W/Mo interfaces are obtained in a column for each growing step and despite the ϕ rotation (dark-field STEM image in Fig. 3b). Assuming the complete miscibility of tungsten and molybdenum, one could expect a more mixed region at W/Mo interfaces. However, the growth front produced by GLAD co-sputtering strongly depends on the shadowing phenomenon and, thus on the geometry of the deposition system. Assuming the column width w (about 150 nm from Fig. 3) and deposition angle ($\alpha_W = \alpha_{Mo} = 80°$), the calculated interface width is $\Delta = 26$ nm[21]. This value is overestimated since sharper vertical interfaces are evidently observed in several W/Mo columns as shown from dark-field STEM (Fig. 3b). In addition, the quality of W/Mo interfaces is connected to diffusion phenomena at grain boundary. Since grain boundary misorientations may occur between W and Mo metals, such misorientations significantly affect diffusivity of Mo in W (and reciprocally), and thus the sharpness of interfaces[26].

Fast-Fourier transform (FFT) patterns obtained from c, d and e zones of the column (Fig. 3c, d and e) correspond to similar [001] bcc zone axes with a <110> growth direction. Since W and Mo both adopt the same bcc crystallographic structure with similar lattice constants (0.3165 nm and 0.3147 nm for W and Mo, respectively), patterns do not allow identifying each metal in columns. However, it is possible to discriminate between them with EDX points performed locally at the nanoscale. Thus, both W and Mo crystallized parts mainly exhibit the [001] orientation corresponding to the α phase with a <110> growth direction. Close to the substrate, the first growing stage exhibit a mixture of α- and β-W phases with grains of 5-10 nm. The [001] zone axis is mainly pointed out for the α-W phase (with a few cases of [111] zone axis), whereas for the β-W phase (A15 crystal structure) [001], [212] and [214] zone axes are also observed. As a result, the presence of a major amount of the α-W phase is noticed in GLAD co-deposited W/Mo films. The opposite result is usually reported when W films are prepared by GLAD with a single W target[27]. The β-W phase prevails assuming that while one side of the columns receives W atoms from the target, the opposite one is exposed to residual background oxygen favoring the formation of this non-equilibrium phase. The GLAD co-sputtering process hinders the formation of the β-W phase due to impingement of Mo atoms on the column side opposing the W target. So, except close to the substrate, all studied W and Mo parts are pointed out with bcc phase, and both with the same [001] zone axis and the <110> growth direction. However, these crystallized areas exhibit defects (dislocations, stacking faults).

The component separation is even more brought to the fore when focuses on the cross-section and top view of the column apex (Fig. 4).

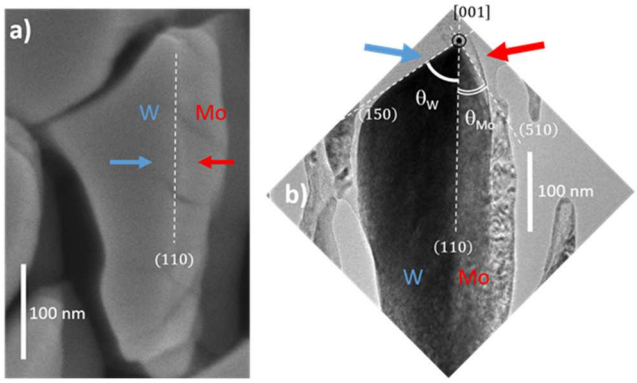

Fig. 4. a) Top view by SEM and b) cross-section observation by TEM of a W-Mo column apex.

The presence of angular facets is particularly marked in the W part of the tip. Despite inaccuracy associated with measuring the facet angle from a cross-section picture, the angle between W/Mo interface and W facet plane (θ_W in Fig. 4b) is 56±2°, where those between W/Mo interface and Mo facet plane (θ_{Mo} in Fig. 4b) is 34±2°. From FFT patterns, the W/Mo interface is made of (110) planes (dashed line in Fig. 4a). Knowing the angle between W/Mo interface and W facet plane (θ_W = 56±2°) and assuming the denser atomic planes, the angular facet of W part observed on the column apex corresponds to (-150) planes. Similarly, the smaller faceted Mo part matches with (510) planes (Fig. 4b). Summing θ_W and θ_{Mo} leads to a right angle, which agrees with (510) being perpendicular to (-150). These three lattice planes ((110), (510) and (-150)) have the [001] common zone axis. The latter correlates with a growth boundary between W and Mo perpendicular to the particle fluxes, as shown in Fig. 4a. The large faceted W part of the column apex appears dense and smooth, whereas cracks and defects are produced in the narrow Mo part. Since W flux prevails (W heavier than Mo), and based-on that no mechanism restrains the transverse growth of the column cross-section, W atoms impinge on a flat and dense tip of columns favoring a fan-like surface morphology due to shadowing effect. Mo atoms depositing on the opposite side of the columns are thus influenced by the fanning and dense structure of W leading to the same bcc crystal structure and the same <110> growth direction.

4. Conclusion

W/Mo vertical columns exhibiting a checkerboard-like structure are prepared by dual-source GLAD co-deposition. W and Mo targets are sputtered with the same tilt angle α_W = α_{Mo} = 80° while the azimuthal angle ϕ of the substrate is periodically changed following sequential 180° ϕ rotations. This well-controlled procedure leads to clear and organized W/Mo alternations with frank interfaces in vertically grown columns. Predominance of the W flux gives rise to asymmetric column profiles. An anisotropic morphology of the column cross-section is also produced like in GLAD films prepared with a single source. Fanning and chaining phenomena of the cross-sections in the direction perpendicular to the particle fluxes are similarly obtained. However, the two-component characteristic stretches out of the column axis and the column apex displays a sharped tip with a large and smooth W faceted zone (facing W target) adjoined with a cracked and defective Mo part (facing Mo target). Both metallic parts correspond to the growth of well-defined crystallographic planes of W and Mo.

These results prove that the GLAD co-sputtering process provides an innovative tool to create original nanostructured systems made of two miscible components prepared on silicon substrates. They also demonstrate that the implementation of two separate sputtering sources can be managed to go well beyond the classical single-component GLAD process. This co-deposition approach extends the range of achievable nanostructures based-on Janus-like architecture and can be broadened to ceramics, semiconductors for applications involving thin film engineering.

5. Acknowledgments

This work has been supported by the Region Bourgogne Franche-Comté and by EIPHI Graduate School (Contract ‘ANR-17-EURE-0002’).

6. References

1. E. Amstrong *et al.*, *ACS Appl. Mater. Interfaces* **7(48)** 27006 (2015).
2. Y. Gong *et al.*, *Adv. Funct. Mater.* **24** 125 (2013).
3. K. Gregorczyk and M. Knez, *Prog. Mater. Sci.* **75** 1 (2016).
4. Y.P. Zhao *et al.*, *Proc. SPIE* **5219** 59 (2003).
5. S.H. Chen *et al.*, *Optic Express* **17(26)** 24153 (2009).
6. C.V. Ramana *et al.*, *ACS Appl. Nano Mater.* **3(4)** 3264 (2020).
7. I. Shtepliuk *et al.*, *ACS Appl. Nano Mater.* **4(2)** 1282 (2021).
8. K. Jefimovs *et al.*, *Microelectron. Eng.* **78-79** 448 (2005).
9. D. Kosters *et al.*, *ACS photonics* **4(7)** 1858 (2017).
10. J. Yan *et al.*, *Nature* **491(7425)** 578 (2012).
11. G. Renaud *et al.*, *Science* **300(5624)** 1416 (2003).
12. Q.F. Guan *et al.*, *ACS Materials Lett.* **3(2)** 243 (2021).
13. K. Robbie and M.J. Brett, *J. Vac. Sci. Technol.* **15(3)** 1460 (1997).
14. A. Barranco *et al.*, *Progr. Mater. Sci.* **76** 59 (2016).
15. M.M. Hawkeye *et al.*, *Glancing angle deposition of thin films: Engineering the nanoscale*, Wiley, Chichester, 2014.

16. M.T. Taschuk *et al.*, in *Handbook of Deposition Technologies for Films and Coatings*, Elsevier, Ed. P.M. Martin, 2010, pp. 621–678.
17. S.V. Kesapragada *et al.*, *Nano Lett.* **6(4)** 854 (2006).
18. H.G. Moon *et al.*, *Sci. Rep.* **2** 588 (2012).
19. Y. Lui *et al.*, *Nat. Comm.* **6** 7043 (2015).
20. C.M. Zhou *et al.*, *Thin Solid films* **517** 124 (2008).
21. C.M. Zhou *et al.*, *Small* **4(9)** 1351 (2008).
22. A. Mardare *et al.*, *Appl. Surf. Sci.* **499** 143943 (2020).
23. R. El Beainou *et al.*, *Mater. Today Commun.* **27** 102331 (2021).
24. R. El Beainou *et al.*, *Mater. Lett.* **264** 127381 (2020).
25. T. Karabacak *et al.*, *J. Vac. Sci. Technol.* **A22(4)** 1778 (2004).
26. Y. Hao *et al.*, *J. Alloy. Compd.* **819** 152975 (2020).
27. R. Krishnan *et al.*, *Nanotechnology* **20** 465609 (2009).